



OPEN Study on variation law of rock mass dilatancy and stress threshold during loading and unloading

Yanhong Du[✉], Laigui Wang, Feng Chen & Kaixing Wang

In order to further understand the dilatancy phenomenon of rock, the conventional triaxial compression test and unloading confining pressure test are carried out with coarse sandstone, and the rock sample underwent single slope shear failure, and the deviatoric stress-strain curve of rock sample without confining pressure is obtained. Combined with the deviatoric stress-axial strain curve, the rock dilatancy process is divided into linear elastic stage, slow relative dilatancy stage, accelerated relative dilatancy stage and absolute dilatancy stage. The concepts of narrow dilatancy (absolute dilatancy) and generalized dilatancy (relative dilatancy) are proposed, and the fracture evolution law of different dilatancy stages is analyzed by numerical simulation. According to the bilinear dilatancy model, the general rules of apparent dilatancy angle and dilatancy index are analyzed. The results show that the apparent dilatancy angle in the conventional triaxial compression test decreases from 66.12° to 39.15°, with a decrease rate of 40.79%; the apparent dilatancy angle decreased from 63.44° to 48.22° in the unloading confining pressure test, with a decrease rate of 23.99%; and the confining pressure of 15 MPa is the demarcation point of the dilatancy index. In both tests, the characteristic stress thresholds (crack initiation stress σ_{ci} , damage stress σ_{cd} , peak strength σ_p) increased with the increase of confining pressure. The dilatancy strain at different dilatancy stages decreases as the confining pressure increases, and the volume strain after unloading confining pressure is greater than that after the conventional triaxial loading. The phenomenon of rock dilatancy mainly occurs in the accelerated relative dilatancy stage and the absolute dilatancy stage, and the proportion of volume strain in the two stages is 76.73%. The research results provide an effective method for analyzing the phenomenon of rock dilatancy.

Keywords Conventional triaxial loading, Unloading confining pressure, Coarse sandstone, Dilatancy, Stress threshold

Rock dilatancy (also known as shear expansion or compression expansion) is an obvious inelastic volume increase phenomenon that occurs in rocks under load before their failure, and it is a universal property of rocks^{1–3}. In 1885, Reynolds observed the dilatancy phenomenon in wet sand for the first time in history⁴. In 1949, Bridgman observed the phenomenon of inelastic volume increase before rock failure in the compression test of talc, marble and diabase, that is, rock dilatancy phenomenon⁵. In 1989, Chen Zongji pointed out that the main reason for the inward movement and damage of the surrounding rock in the mine roadway was the rock dilatancy caused by the deviatoric stress⁶. It can be seen that the failure of roadway surrounding rock is related to rock dilatancy, and the study of rock dilatancy can further understand the deformation mechanism of roadway surrounding rock.

The magnitude and rate of rock dilatancy are related to the type of rock and the external load it receives^{7–17}. Ping et al.¹⁸ studied that the volume strain of fractured rock mass decreased with the increase of confining pressure under different confining pressures, and indicated that volume strain was the main cause of the convergence deformation of roadway surrounding rock. Meng et al.¹⁹ studied the characteristics between the strength and dilatancy of rocks under different confining pressure cyclic loading and unloading conditions and found that the greater the confining pressure, the smaller the shear expansion angle. Xu et al.²⁰ studied the influence of the number of cycles on the volume strain of salt rocks under triaxial cyclic loading. Lu et al.²¹ proposed the dilatancy-fragmentation failure process of sandstone described by characteristic stress. Zhao et al.²² studied the damage and dilatancy characteristics of deep granite in the Beishan preselection area of the geological disposal depot for high-level radioactive waste in China under the triaxial cyclic loading and unloading conditions. Hou

School of Mechanics and Engineering, Liaoning Technical University, Fuxin 123000, Liaoning, China. ✉email: duyanhong1209@sina.com

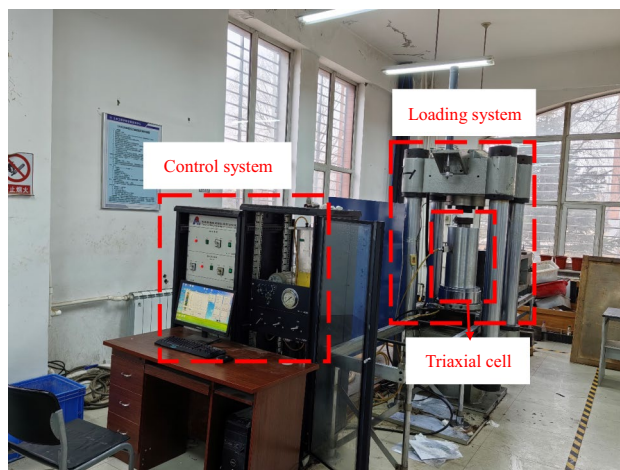


Fig. 1. TAW-2000 microcomputer controlled electro-hydraulic servo rock triaxial testing machine.

Parameter name	Value
Maximum test force	2000 kN
Measurement accuracy	$\pm 0.25\%$
Displacement range	0–100 mm
Displacement Measurement resolution	0.001 mm
Maximum confining Pressure	150 MPa
Confining pressure Resolution	0.05 MPa
Axial deformation	0–10 mm
Lateral deformation	0–5 mm
Displacement Measurement resolution	0.0001 mm

Table 1. Technical parameters of TAW-2000 microcomputer controlled electro-hydraulic servo rock triaxial testing machine.

et al.²³ qualitatively described the characteristics of the volume stress-axial strain curve of rocks. Zhang et al.²⁴ through the uniaxial compression test and pseudo-triaxial test of the cryptocrystalline basalt from Baihetan, pointed out that its dilatancy characteristics can be described by the ratio of the instantaneous dilatancy angle to the internal friction angle. Li et al.²⁵ determined the initiation stress and crack damage stress of shale based on the inflection points of crack volume strain and rock sample volume strain, respectively. Huang et al.²⁶ conducted unloading tests on the green mudstone sandstone of Jinping Hydropower Station and established a constitutive model reflecting the rock dilatancy characteristics under unloading conditions. Liu et al.²⁷ analyzed the mechanical response and dilatancy characteristics of the marble under four stress paths and proposed a new empirical dilatancy coefficient based on the energy dissipation method.

The above-mentioned research has revealed the variation laws of stress, damage and dilatancy of different types of rocks under different loads from different perspectives, and has achieved research results of certain value. Based on previous studies, this paper conducts conventional triaxial compression tests and unloading confining pressure tests on coarse sandstone. The rock volume strain curve is used to divide the rock dilatancy into four stages, and the characteristics of each dilatancy stage of the rock are discussed in detail. The concepts of volume strain and dilatancy are distinguished, and the stress threshold of coarse sandstone is determined in combination with the rock expansion behavior of the rock. The relationship between dilatancy index and confining pressure under different loading methods is analyzed.

Experimental design

Laboratory test

Test equipment and specimens

(1) Test equipment

The uniaxial compression test, conventional triaxial compression test and unloading confining pressure test of coarse sandstone were carried out by using the TAW-2000 microcomputer-controlled electro-hydraulic servo rock triaxial testing machine (as shown in Fig. 1). The technical parameters of this equipment are shown in Table 1. The triaxial pressure chamber adopts a self-balancing pressure chamber, which ensures that

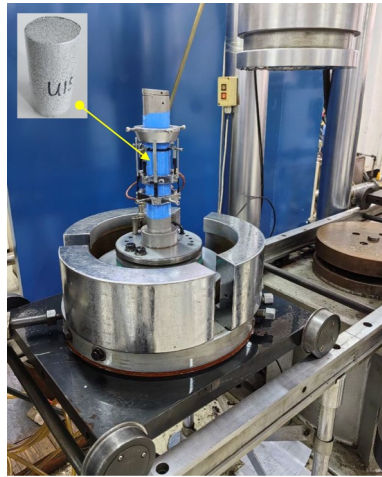


Fig. 2. Installation of rock sample, axial extensometer and lateral extensometer.

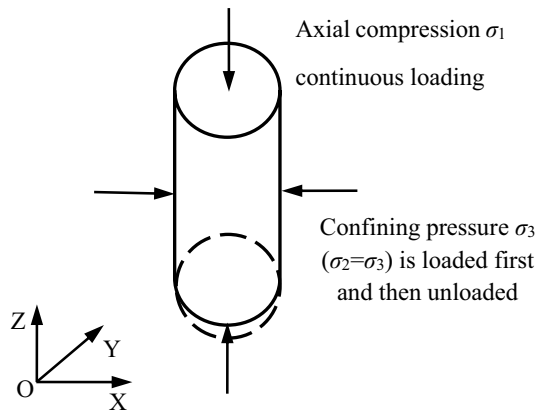


Fig. 3. Stress path in unloading confining pressure test.

the pressure on the rock in all directions is the same when no axial pressure is applied. Moreover, when axial pressure is applied, the confining pressure exerts no additional force on the axial pressure. The rock sample, axial extensometer and lateral extensometer are all located in the triaxial pressure chamber. Each part of the upper and lower pressure heads and the entire wrapped rock sample are re-wrapped in the blue heat shrink tube to prevent eccentric compression. The axial extensometer and the lateral extensometer are used to measure the deformation, as shown in Fig. 2.

(2) Rock samples

In this experiment, coarse sandstone was used to make standard cylindrical rock samples with a diameter \times height of 50×100 mm. The non-parallelism error of both ends of each rock sample is not more than 0.005 mm, and the error along the height and diameter of the rock sample is not more than 0.3 mm. The density of the rock sample is 9.025 g/cm^3 . All rock samples are taken from the same batch of light gray coarse-grained sandstone. Because of its good integrity, uniform material, no impurities and no visible cracks, the internal structure of all rock samples is approximately the same. The comparative analysis of the test results under different confining pressures using this batch of rock samples is reliable. The rock samples are wrapped with transparent heat shrink tubes with a shrinkage ratio of 2:1 to prevent rock fragments from popping out due to sudden rock failure during the test, so as to ensure the integrity and the safety of the experiment of the rock samples after failure. The heat shrinkable tube is contracted with a hot air gun.

Indoor test scheme

In the unloading confining pressure test, a reasonable stress path can simulate the stress state of rock mass in practical engineering. The selection of stress path is of great significance to study the dilatancy and crack evolution laws of coarse sandstone, and for clarifying the macroscopic failure mechanism of coarse sandstone. Figure 3 shows the loading process of the unloading confining pressure test, and the specific unloading test steps are as follows.

The first step: Determine the triaxial compressive strength of the rock sample under different confining pressures. In the test, the increment of confining pressure σ_3 was 0.1 MPa, which increased to 5, 10, 15, 20 and 25 MPa respectively. The axial pressure σ_1 (with an increment of 100 N) was continuously loaded until the rock sample failed.

The second step: Apply axial pressure and set confining pressure. Axial and confining pressures are applied to the rock sample in the loading method of the first step, and the loading reaches 70% of the triaxial compressive strength corresponding to the confining pressure, which is equivalent to simulating the reserve process of strain energy in the rock mass.

The third step: Apply axial pressure and relieve confining pressure before peak. Reduce the confining pressure at a rate of 0.1 MPa/s, and simultaneously increase the axial pressure at a rate of 100 N/s until the rock sample is damaged.

In the conventional triaxial loading test, the rock samples were marked as C0, C5, C10, C15, C20, and C25 respectively. In the unloading confining pressure test, the rock samples were marked as U5, U10, U15, U20, and U25 respectively. The numbers represent the corresponding confining pressure values. The conventional triaxial loading test scheme is the same as the first step of the unloading confining pressure test.

Numerical simulation

RFP software is used to simulate the conventional triaxial compression test and unloading confining pressure test. The numerical simulation parameters are shown in Table 2. Using RFP software for numerical simulation, it is necessary to convert the uniaxial compressive strength and elastic modulus obtained from laboratory tests into the input values of the numerical simulation. The specific conversion methods are shown in Formulas (1) and (2).

$$\frac{f''}{f'} = 0.2602 \ln m + 0.0233(1.2 \leq m \leq 50) \quad (1)$$

$$\frac{E''}{E'} = 0.1412 \ln m + 0.6476(1.2 \leq m \leq 50) \quad (2)$$

In the formula: E' and f' represent the elastic modulus and uniaxial compressive strength of the numerical simulation input respectively; E'' and f'' are the elastic modulus and uniaxial compressive strength obtained from the uniaxial compression test, respectively. The m is the uniformity coefficient of the rock, and its physical meaning reflects the uniformity of the rock medium. The larger m is, the better the degree of uniformity of the rock.

The size of the numerical model is 50×100 mm, and the number of divided elements is 100×200 . The specific numerical simulation parameters are shown in Table 2. The increment of the axial load was 0.005 mm in the numerical simulation, and other loading methods were the same as those in the laboratory test.

Overview of stress–strain curve

The complete stress-strain curve of rock can reveal the strength and deformation characteristics of rock. In general, according to the total stress-strain curve of rock, the deformation stages of rocks can be divided by the following two methods. The first method divides rock deformation into five stages (see Fig. 4): ① pore and fracture compaction stage *OA*, ② linear elasticity stage *AB*, ③ crack stable development stage *BC*, ④ crack unstable development stage *CD*, ⑤ failure stage *DE*. The second method divides the rock deformation into four stages, namely, merging stage ③ of crack stable development and stage ④ of crack unstable development and collectively referring to them as the plastic stage *BD*, while the names of the remaining stages remain unchanged. This article adopts the first classification method.

The deformation and failure process of rock is accompanied by the closure, initiation, expansion and penetration of cracks. The whole process of rock deformation and failure is divided into five stages by four characteristic stress thresholds^{1,28–31}. The four characteristic stress thresholds are respectively the crack closure stress σ_{cc} at point A, the crack initiation stress σ_{ci} at point B, the crack damage stress σ_{cd} at point C, and the peak strength σ_p at point D. Furthermore, the residual strength σ_r corresponding to point E.

The deviatoric stress-strain curves of different rock samples obtained by uniaxial compression test, conventional triaxial compression test and unloading confining pressure test of coarse sandstone are shown in Figs. 5 and 6. The fracture forms of each rock sample were all single-slope shear failure (see Figs. 7 and 8). The rock samples are relatively hard and have no cracks. The deviatoric stress-axial strain curves of the rock samples show no obvious pore and crack compaction stages. The crack closure stress σ_{cc} is not considered for the time being. The crack damage stress σ_{cd} , which is the boundary point between the stable development stage and the unstable development stage of the crack, can not be clearly determined only by the deviatoric stress-axial strain

Parameter name	Value	Parameter name	Value
Homogeneity	5	Poisson's ratio	0.25
Elastic modulus(MPa)	3570	Density(g/cm ³)	2.155
Strength(MPa)	44.32	Friction angle(°)	30

Table 2. Numerical simulation parameters.

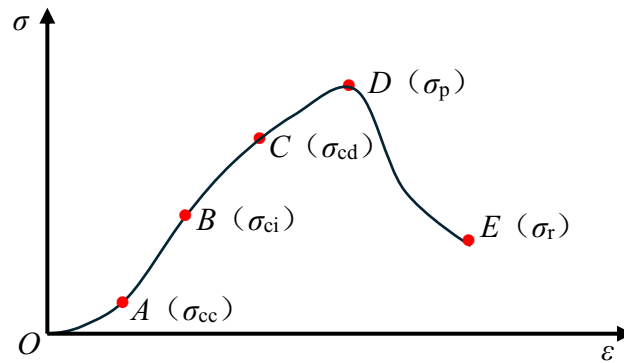


Fig. 4. Rock complete stress-strain curve diagram and characteristic stress threshold.

curve, and the crack damage stress σ_{cd} can be determined by the volume strain curve. The variation trend of the lateral strain curve and the determination method of the characteristic stress threshold are not elaborated on the axial strain curve.

At present, the stage division of the stress-axial strain curve, the curve characteristics of each stage and the crack evolution law have been described in detail, but the volume strain curve has not been comprehensively and clearly described.

Volume strain and dilatancy

The concept and calculation of volume strain

The rate of volume change per unit volume of rock is called volume strain ε_v , abbreviated as volume strain.

At present, the volume strain can not be directly measured in the rock mechanics test, which can be calculated according to the following formula.

$$\varepsilon_v = \frac{1 - 2\nu}{E} I_1 \quad (3)$$

Where E is the elastic modulus; ν is Poisson's ratio; $I_1 = \sigma_x + \sigma_y + \sigma_z = \sigma_1 + \sigma_2 + \sigma_3$, which is the first invariant of the stress tensor; σ_x , σ_y and σ_z are the normal stresses along the x , y , and z directions respectively; σ_1 , σ_2 and σ_3 are respectively the maximum principal stress, the intermediate principal stress and the minimum principal stress, which are also respectively called the first principal stress, the second principal stress, and the third principal stress. This formula is derived from the theory of elastic mechanics, so it is only applicable to the linear elastic stage of rock deformation, and can only draw the deviatoric stress-volume strain curve of the linear elastic stage of rock.

Because formula (3) is not applicable to the crack stable development stage, crack unstable development stage and failure stage of rock deformation, the following method is adopted in this paper to calculate the volume strain, and the deviatoric stress-strain curves of the entire process of rock deformation and failure in the conventional triaxial compression test and unloading confining pressure test are respectively drawn (see Figs. 5 and 6).

Let there be cubic element bodies with edge lengths dx , dy and dz , and their volumes are.

$$V = dxdydz \quad (4)$$

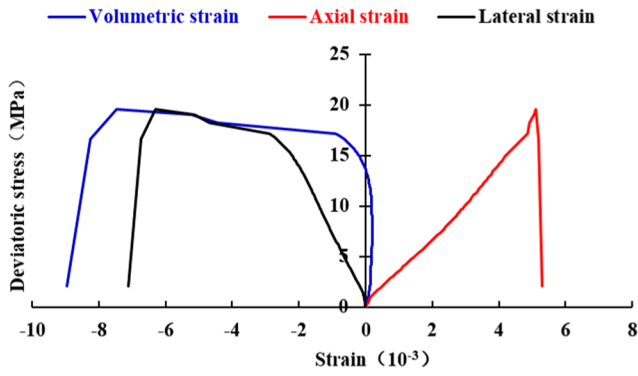
After the rock mass is deformed under force, the edges of each element are elongated or shortened, and the included angles between adjacent edges are also changed. The volume change caused by shear strain is a high-order micro-quantity, so it is neglected. In addition, the high-order micro-amount of linear strain is also neglected²⁶⁻²⁸. Then the volume of the deformed unit body is

$$V' = (1 + \varepsilon_x)dx(1 + \varepsilon_y)dy(1 + \varepsilon_z)dz \approx (1 + \varepsilon_x + \varepsilon_y + \varepsilon_z)dxdydz \quad (5)$$

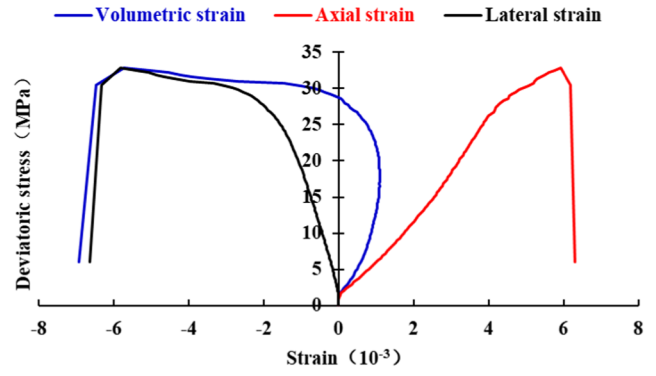
The volume strain is

$$\varepsilon_v = \frac{V' - V}{V} = \varepsilon_x + \varepsilon_y + \varepsilon_z = \varepsilon_1 + \varepsilon_2 + \varepsilon_3 = \varepsilon_1 + 2\varepsilon_3 \quad (6)$$

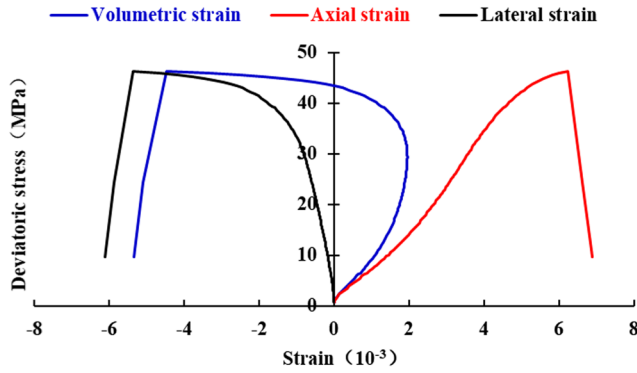
In the formula: ε_x , ε_y and ε_z are the linear strains in x , y , z direction respectively; ε_1 , ε_2 and ε_3 are the maximum, middle and minimum principal strains, respectively. In the rock mechanics test, ε_1 (ε_x) represents axial strain, ε_2 (ε_y) and ε_3 (ε_z) represent the uniform lateral strain, and in conventional triaxial compression tests, $\varepsilon_2 = \varepsilon_3$. According to the regulations of rock mechanics, compression is positive and expansion is negative. Therefore, the axial compressive strain is positive and the lateral expansion strain is negative. When ε_v is greater than zero, the rock sample shrinks, and When ε_v is less than zero, the rock sample expands. If ε_v is zero at each point in the



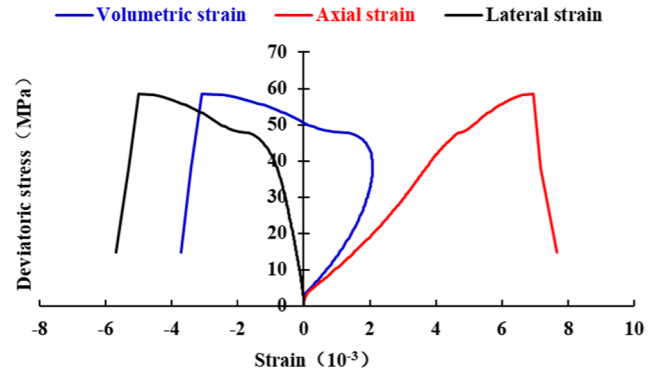
(a) Rock specimen C0



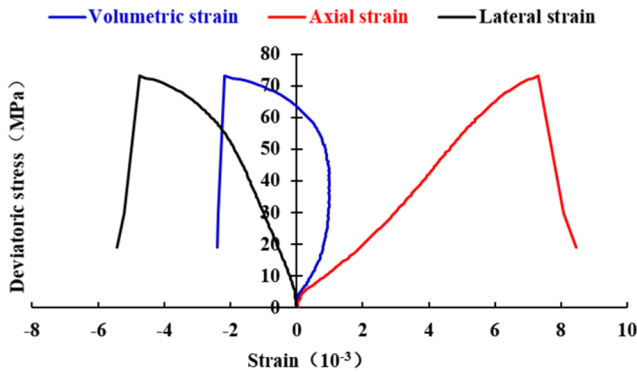
(b) Rock specimen C05



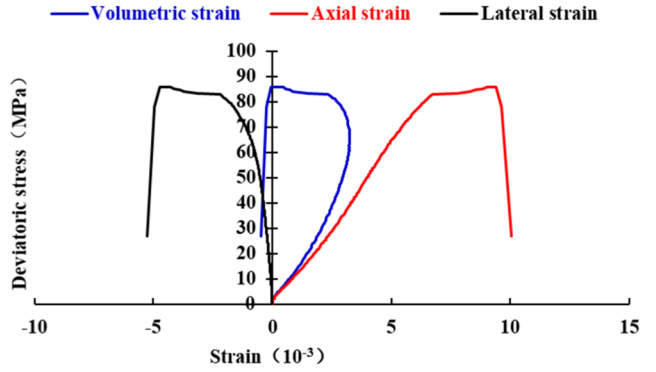
(c) Rock specimen C10



(d) Rock specimen C15



(e) Rock specimen C20



(f) Rock specimen C25

Fig. 5. The deviatoric stress-strain curve of rock specimen under conventional triaxial loading test. The confining pressure of rock specimen C0 in the (a) is 0, which is the result of uniaxial compression test (a).

object, it indicates that the shape of the object changes after the force is applied, and the volume does not change, which is called is volume deformation³².

Volume strain curve division and different dilatancy stages

According to the different deformation stages of the rock, the volume strain can be calculated by formula (4). The volume strain curves of rocks in the conventional triaxial loading test and unloading confining pressure test can be divided into the following four stages. In this paper, the rock sample C10 is taken as an example, and the various stages of the rock volume strain curve are explained in detail in combination with Fig. 9.

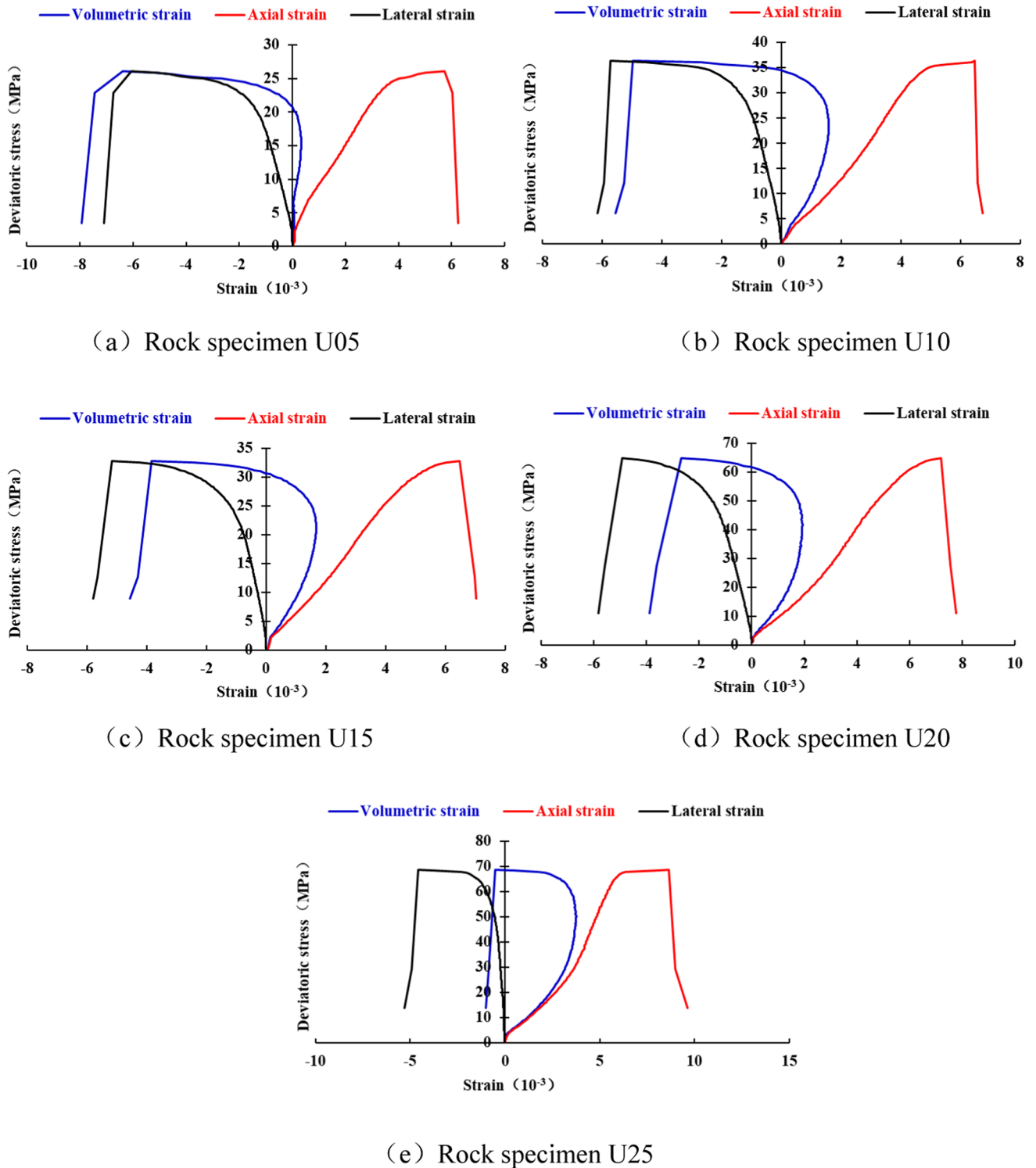


Fig. 6. The deviatoric stress-strain curve of rock specimen in unloading confining pressure test.

- (1) Linear elastic stage OB' . The volume strain increases linearly with the increase of deviatoric stress in the linear elastic stage, that is, the two are proportional. Because the axial compressive strain is greater than the sum of the expansion strain on both sides, that is $\epsilon_1 > |\epsilon_2 + \epsilon_3|$, the volume of the rock sample decreases with the increase of the deviatoric stress in this stage, and it is in a compressive state.

The linear elastic stage of the deviatoric stress-volume strain curve corresponds to the linear elastic stage of the deviatoric stress-axial strain curve, and the deviatoric stress value at the highest point of the linear elastic stage

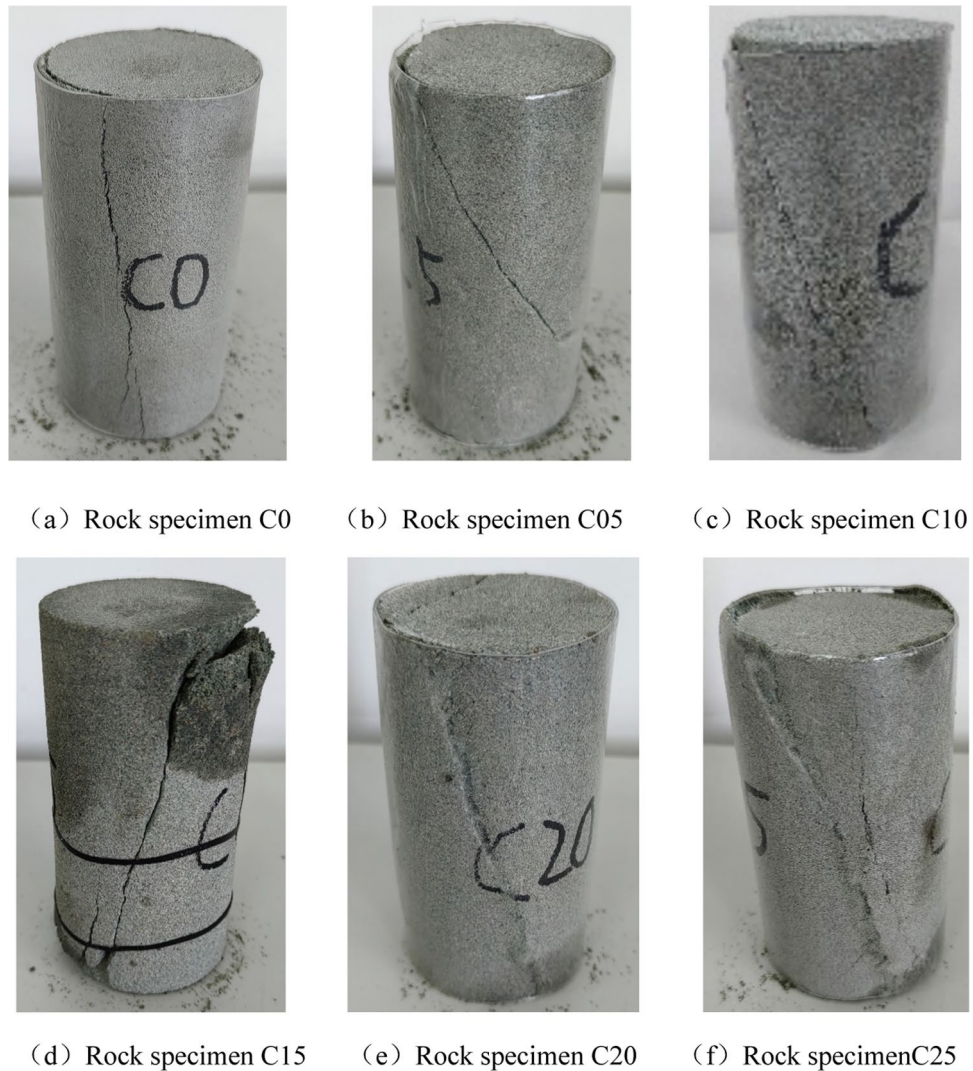


Fig. 7. Failure mode of rock specimen in conventional triaxial loading test.

of the deviatoric stress-volume strain curve corresponds to the crack initiation stress σ_{ci} in the characteristic stress threshold.

- (2) Slow relative dilatancy stage $B'C'$. When the deviatoric stress is greater than σ_{ci} , the deviatoric stress-volume strain curve begins to bend to the left and deviates from the original straight line. The degree of this deviation increases with the increase of the deviatoric stress, that is, the length of the line segment KK' becomes larger and larger. This phenomenon leads to a reduction in the volume compression of the rock body at this stage compared to the ideal linear elastomer (as shown by the imaginary straight line in Fig. 9), and the part deviating from the linear elasticity (KK') represents the relative volume reduction. Conversely, the length of the line segment KK' represents a nonlinear increase in the volume of the rock relative to the ideal linear projectile. Therefore, point B' is called the starting point of rock dilatancy. During the $B'C'$ stage, the slope of the volume strain curve gradually decreases, and the rate of increase in relative dilatancy capacity gradually slows down, this stage is called the slow relative dilatancy stage.

The inflection point C' indicates that the absolute volume compression of the rock reaches its peak, and the rock volume is the smallest at this point. In the neighborhood of the inflection point C' , the volume strain varies with the deviatoric stress, but the increment of volume strain is approximately zero, and the volume size of the rock hardly changes. It is worth noting that the absolute volume of rock samples in this stage still decreases with the increase of deviatoric stress, which is in a compressive state, and the volume strain increment gradually decreases. It is only that compared with the ideal linear elastomer, the volume is relatively increased.

The slow relative dilatancy stage of the deviatoric stress-volume strain curve corresponds to the crack stable development stage of the deviatoric stress-axial strain curve, and the deviatoric stress of the inflection point C' corresponds to the crack damage stress σ_{cd} in the characteristic stress threshold.



(a) Rock specimen U05 (b) Rock specimen U10 (c) Rock specimen U15



(d) Rock specimen U20 (e) Rock specimen U25

Fig. 8. Failure mode of rock specimen in unloading confining pressure test.

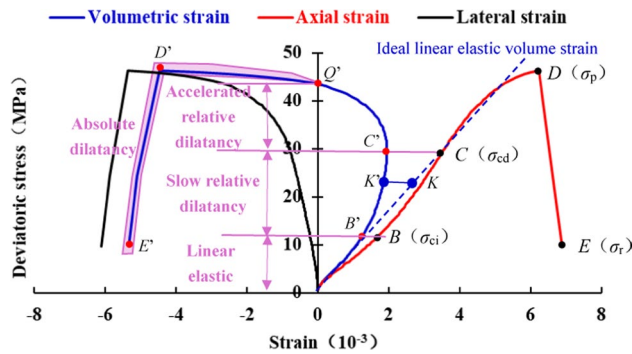


Fig. 9. Volume strain curve stage division and different dilatancy stages.

- (3) Accelerated relative dilatancy stage C'Q'. After the inflection point C', the volume of the rock still shows a nonlinear increase relative to that of the ideal linear projectile. The absolute value of the slope of the volume strain curve gradually increases, and the increase rate of the relative dilatancy capacity gradually accelerates. Therefore, this stage is called the accelerated relative dilatancy stage.

At this stage, the length of KK' gradually increases, and the relative compression of the volume gradually decreases. The volume strain remains positive, and the rock is still relatively dilatancy and absolutely compressed. The absolute volume compression amount gradually decreases.

- (4) Absolute dilatancy stage $Q'E'$. The volume strain is negative, and the axial compressive strain is less than the sum of the expansion strains on both sides, that is, $\varepsilon_1 < |\varepsilon_2 + \varepsilon_3|$, the volume of the rock is no longer shrinking. Compared with the unstressed rock sample, the volume expands, and this phenomenon of obvious increase in volume is called absolute dilatancy. This stage is called absolute dilatancy stage.

The partial $Q'D'$ in the absolute dilatancy stage and the accelerated relative dilatancy stage correspond to the unstable development stage of the crack in the deviatoric stress-axial strain curve, and the deviatoric stress at the highest point D' of the volume strain curve corresponds to the peak strength σ_p in the characteristic stress threshold.

To sum up, the author believes that the concept of dilatancy has two meanings: one is narrow and the other is broad. Narrowly defined dilatancy is absolute dilatancy ($Q'E'$ stage), taking the volume of the unstressed rock as a reference, if the volume of the rock is greater than this reference value during the loading process, the volume strain is negative. In a broad sense, dilatancy is relative dilatancy, also known as dilatancy. Taking the ideal linear elastic volume strain of the rock (as shown by the virtual straight line in Fig. 9) as a reference, the deviation of the volume strain curve from the straight line is regarded as rock dilatancy, including the slow relative dilatancy stage $B'C'$, the accelerated relative dilatancy stage $C'Q'$ and the absolute dilatancy stage $Q'E'$.

Crack evolution laws in different dilatancy stages

Accuracy verification of numerical simulation results

The deformation and failure process of rock during compression process could not be observed in the indoor test. In this paper, the RFPA software was used to simulate the rock fracture process. Taking rock sample C10 as an example, the evolution law of cracks in different dilatancy stages of the rock is described in detail. Figure 10 shows the comparison of the deviatoric stress-axial strain curves between the indoor test and the numerical simulation, and Fig. 11 shows the comparison of the failure mode of rock sample C10 in the indoor test with the numerical simulation results. It can be known through the comparison of curves and failure forms that the numerical simulation has well simulated the fracture process of rock samples in the indoor test, and the numerical simulation results are reliable and accurate.

Fracture evolution law in different expansion stages

The evolution process of rock instability and fracture can be reflected by acoustic emission, and the location of its failure can be located^{29,30}. The blue units in the elastic modulus diagram represent the rock blocks that are about to be broken. In the acoustic emission diagram, the white circles represent shear failure and the red circles represent tensile failure. The larger the circle in the acoustic emission diagram, the greater the energy released when the unit is damaged. A total of 9 groups of shear stress diagrams (left column), elastic modulus diagrams (middle column), and acoustic emission diagrams (right column) were intercepted to comprehensively present the instability and fracture process of the rock sample, as shown in Fig. 12.

The broken rock blocks are scattered within the rock during the line elastic stage of the dilatancy, as shown in the acoustic emission diagram in Fig. 12a, and the failure mode of the rock blocks is shear failure. When the stress is about to reach the crack initiation stress value, there are band-like high-stress areas in the local area of the rock, as shown in Fig. 12b. When the stress reaches the crack initiation stress value, the acoustic emission shows a band-like aggregation phenomenon, and cracks appear in the rock, as shown in Fig. 12c. When the loading continues, the length of the banded crack gradually increases in the slow relative dilatancy stage. At the same time, the banded failure zone also appears in the lower right corner of the rock sample, as shown in Fig. 12d. When the stress reaches the damage stress value, the already manifested banded crack shows radial expansion. This crack can be clearly seen through the shear stress diagram, as shown in Fig. 12e. At the moment following the stress characteristic point C' (damage stress), that is, the stage of accelerated relative dilatancy, the

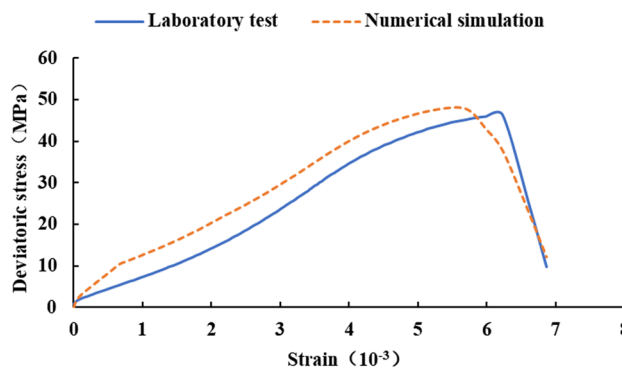


Fig. 10. Comparison of rock sample C10 deviatoric stress-axial strain curves of indoor test and numerical simulation.

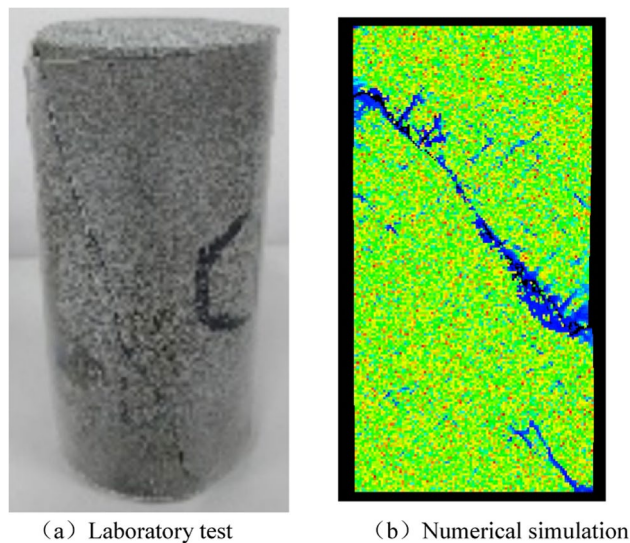


Fig. 11. Comparison of rock sample C10 failure modes of indoor test and numerical simulation.

crack shows unstable expansion, and the crack length is approximately twice that of the previous moment, with the dilatancy accelerating, as shown in Fig. 12f. When the load was applied to point Q', and the crack length has expanded to approximately half of the entire length, and the crack penetrates to the left boundary of the rock sample, as shown in Fig. 12g. As the load reaches the peak strength, both the cracks in the middle of the rock sample and the cracks in the lower right corner of the rock sample continue to expand, but they do not penetrate, and the cracks in the middle of the rock sample do not penetrate into the right boundary of the rock sample (see Fig. 12h), and the rock sample still has a certain bearing capacity. Until the loading was completed, the crack in the middle of the rock sample ran through the right boundary of the rock sample, and at the same time, new secondary cracks appeared on this crack.

Dilatancy indicators

Bilinear dilatancy model

It can be seen from Fig. 13 that the volume strain-axial strain curves of coarse sandstone in the conventional triaxial loading test and unloading confining pressure test can be simplified into two stages with the inflection point as the dividing point (see Fig. 14). The first stage includes the initial elastic shrinkage and slow relative dilatancy of the rock, and the second stage includes the accelerated relative dilatancy and absolute dilatancy of the rock. Figure 14 shows a simplified bilinear model of the volume strain-axial strain curves of rock samples under different loading conditions. This Fig. reflects the relationship between rock dilatancy and confining pressure, and describes the general law followed by rock dilatancy: (1) Rocks exhibit linear elastic shrinkage properties under any test conditions. (2) As the confining pressure increases, the elastic shrinkage of the rock increases, the dilatancy capacity decreases, and the dilatancy phenomenon is delayed. (3) The slopes of both straight lines in the bilinear model gradually decrease as the confining pressure increases, that is, the dilatancy rate (the dilatancy capacity per unit time) decreases.

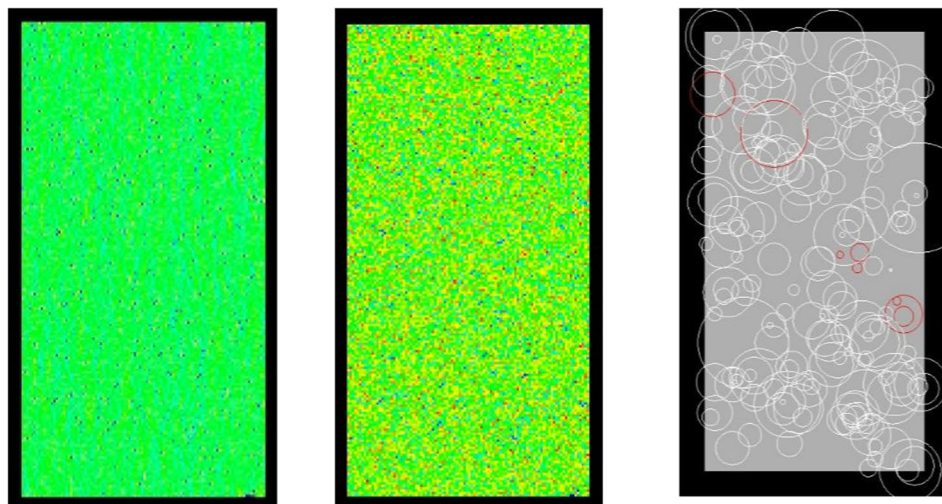
Apparent dilatancy angle and dilatancy index

(1) Apparent dilatancy angle

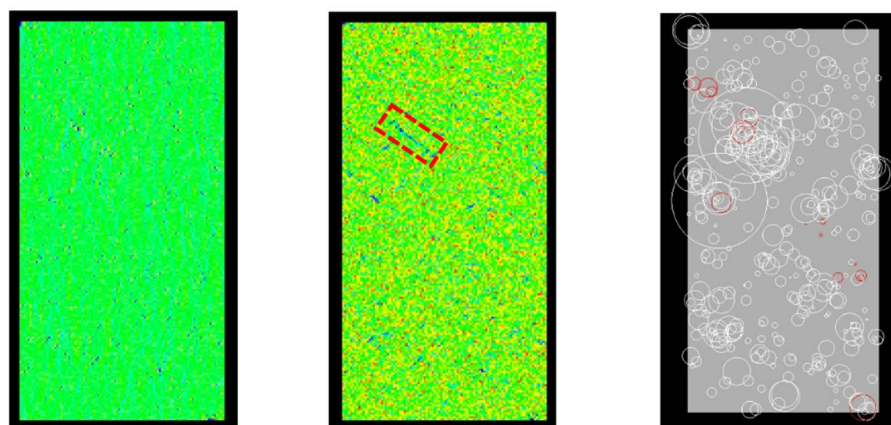
The rock dilatancy parameters—the apparent dilatancy Angle and the dilatancy index - are defined based on the bilinear dilatancy model. The Angle at which the positive slope of the straight line segment of the bilinear dilatancy model makes an angle less than 90° with the horizontal line is defined as the apparent dilatancy angle θ , with the unit of $^\circ$. The dilatancy angle is the largest under uniaxial loading conditions, which can approach 90° [31–34]. The greater the confining pressure, the smaller the rock dilatancy and the smaller the apparent dilatancy angle. The apparent dilatancy angles of different test rock samples are shown in Table 3. When the confining pressure increased from 5 MPa to 25 MPa, the apparent dilatancy angle decreased from 66.12° to 39.15° in the conventional triaxial loading test, which decreases by 26.97° , and the decrease rate is 40.79%. In the unloading confining pressure test, the apparent dilatancy angle decreased from 63.44° to 48.22° , a decrease of 15.22° , with a decrease rate of 23.99%.

(2) Dilatancy index

The dilatancy index reflects the phenomenon that the dilatancy capacity of rocks decreases with the increase of confining pressure. The dilatancy index I_d is defined as the ratio of the apparent dilatancy angle under confining pressure to that under uniaxial compression conditions. The greater the confining pressure is, the smaller the

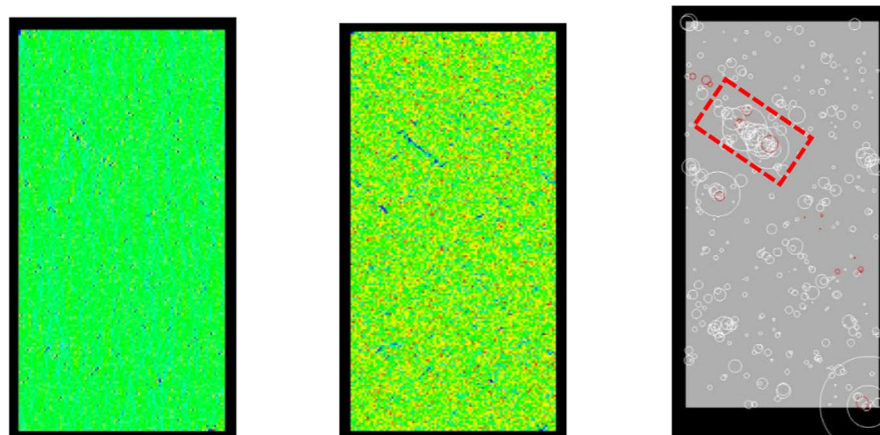


(a) The intermediate moment of the linear elastic phase



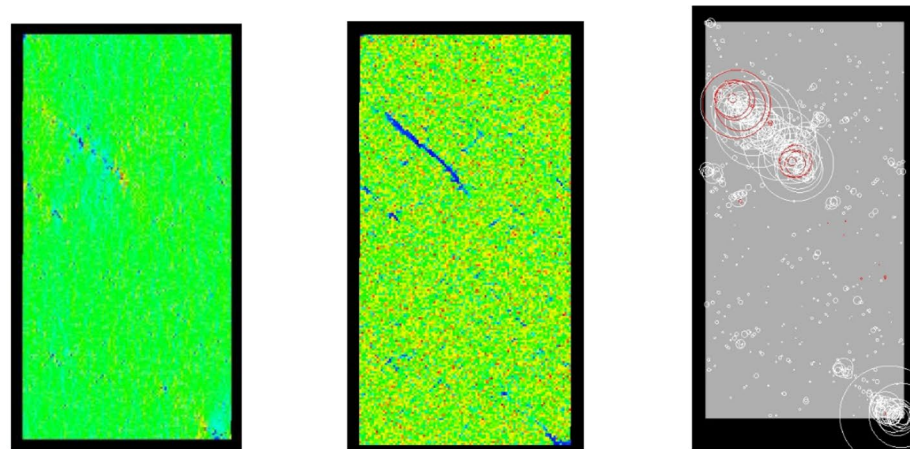
(b) The linear elastic stage at the moment before the stress characteristic point B'

(crack initiation stress)

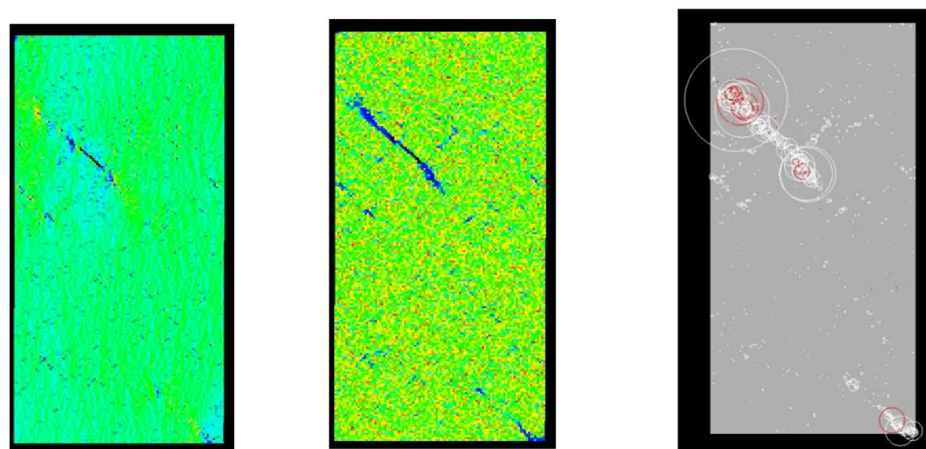


(c) Stress characteristic point B' (Initiation stress)

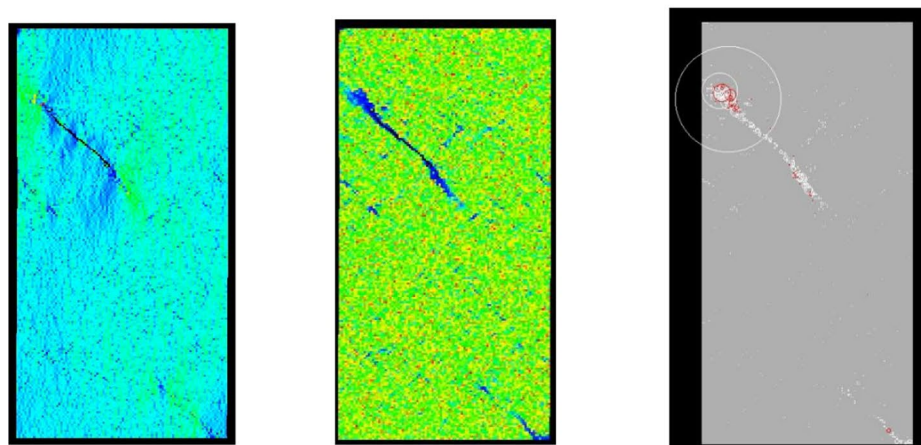
Fig. 12. Rock sample fracture process, the points in (a)–(i) serial number title correspond to the points in Fig. 9.



(d) The stage of slow relative dilatancy at the moment before the stress characteristic point C' (damage stress)



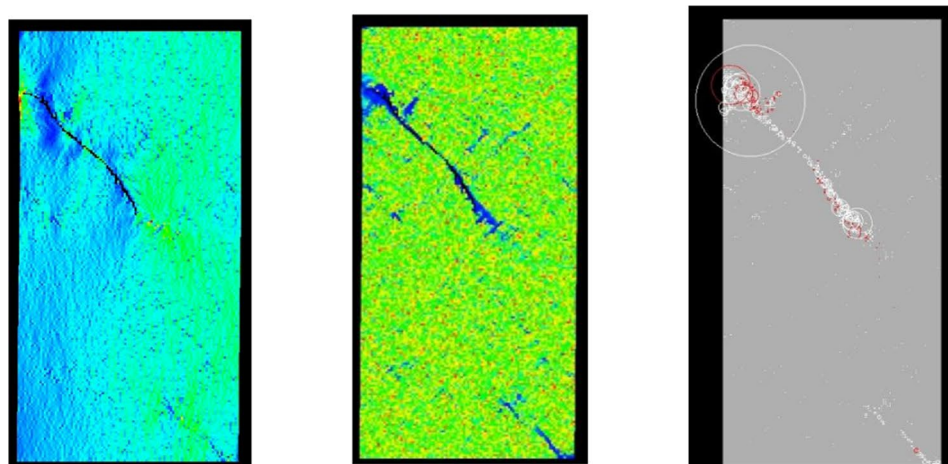
(e) Stress characteristic point C' (damage stress)



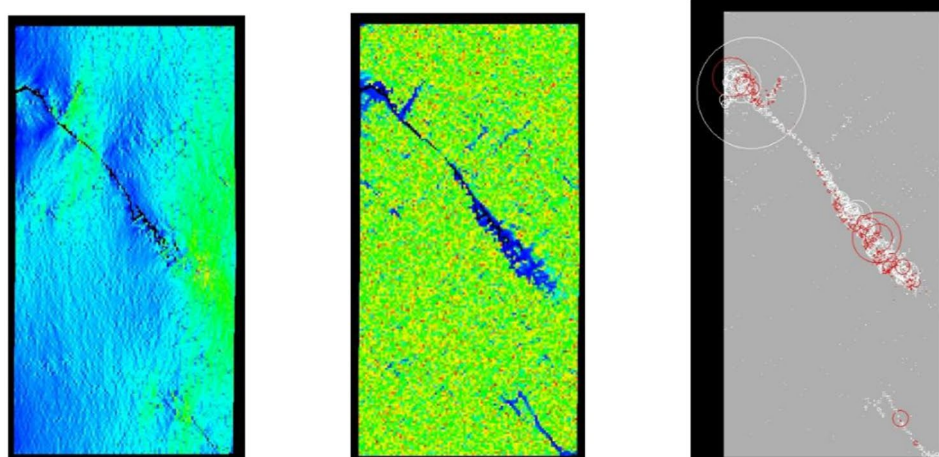
(f) The stage of accelerated relative dilatancy at the moment following the stress characteristic point C' (damage stress)

Fig. 12. (continued)

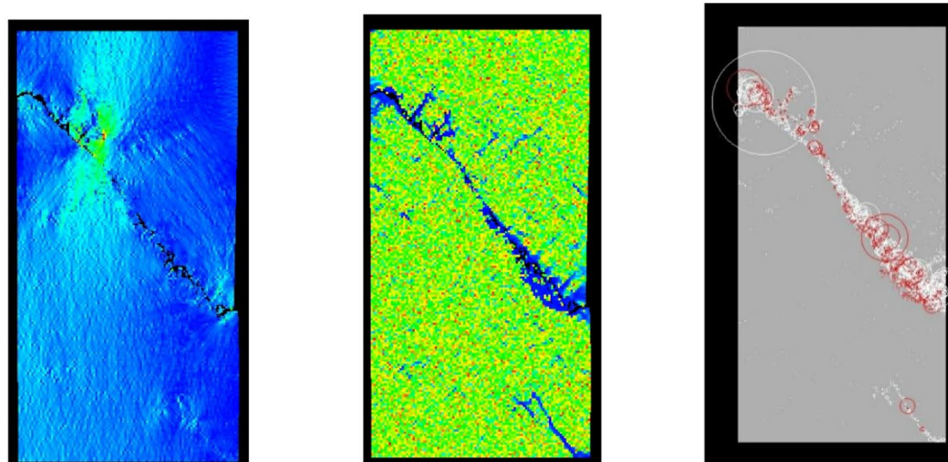
dilatancy index is, the less obvious the dilatancy phenomenon of the rock is, and the smaller the volume of fractures inside the rock is. The definition formula of the dilatancy index I_d is as follows:



(g) Q' point



(h) Stress characteristic point D' (peak strength)



(i) Point E' (Residual strength)

Fig. 12. (continued)

$$I_d = \frac{\theta_p}{\theta_0} = \frac{\arctan(\Delta\varepsilon_{vp}/\Delta\varepsilon_{1p})_p}{\arctan(\Delta\varepsilon_{vp}/\Delta\varepsilon_{1p})_0} \quad (7)$$

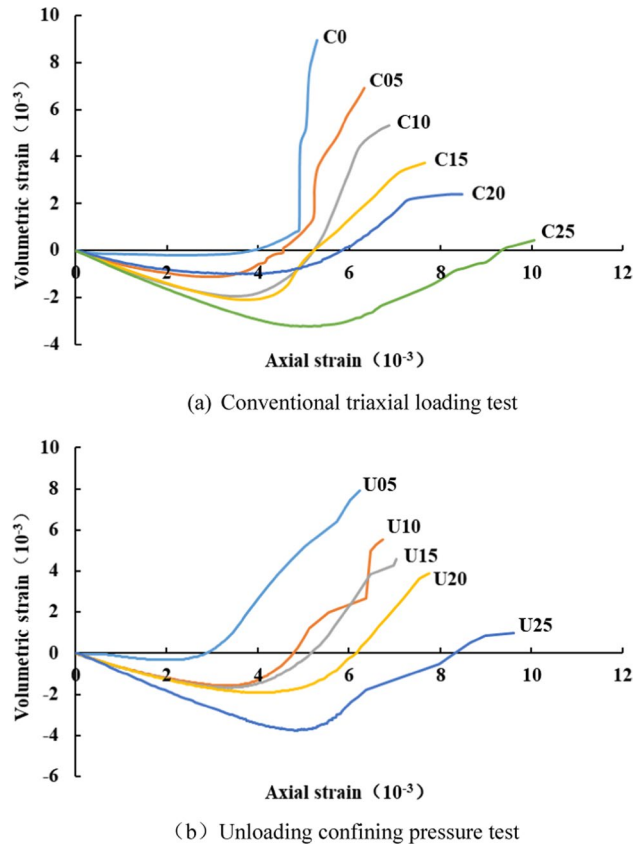


Fig. 13. Volume strain-axial strain curves of different test rock samples.

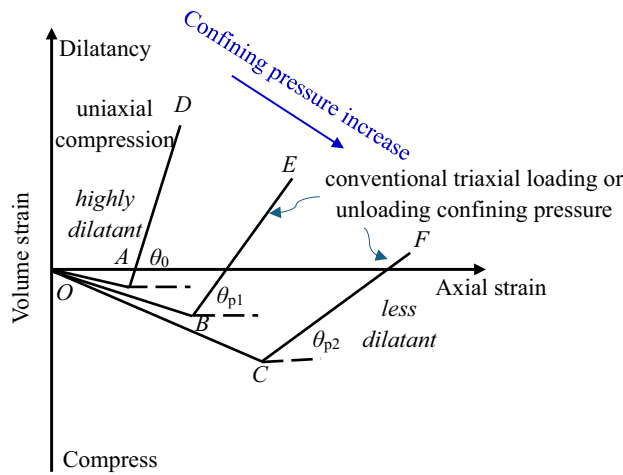


Fig. 14. Bilinear dilatancy model.

Where θ_p represents the apparent dilatancy angle when there is confining pressure; θ_0 represents the apparent dilatancy angle under uniaxial compression conditions; $\Delta\epsilon_{vp}$ increment of plastic volume strain; $\Delta\epsilon_{1p}$ plastic axial strain increment.

The I_d is between 0 and 1. $I_d = 0$ (minimum dilatancy) indicates that the rock has no dilatancy, and $I_d = 1$ (maximum dilatancy) indicates the uniaxial compression situation. The I_d from large to small reflects the transformation of the rock from a high dilatancy state under uniaxial compression to a small dilatancy state under high confining pressure. The specific values of I_d in this experiment are shown in Table 3.

The apparent dilatancy angle and dilatancy index can be calculated from the measurement to the test data by using Eq. (7), and then the dilatancy properties of various rocks in different environments can be determined.

Confining pressure(MPa)	Conventional triaxial loading test		Unloading confining pressure test		Dilatancy index difference
	Apparent dilatancy angle $\theta(^{\circ})$	Dilatancy index I_d	Apparent dilatancy angle $\theta(^{\circ})$	Dilatancy index I_d	
0	73.09	1	—	—	—
5	66.12	0.90	63.44	0.87	0.03
10	64.87	0.89	62.88	0.86	0.03
15	59.76	0.82	58.45	0.80	0.02
20	39.44	0.54	55.75	0.76	0.22
25	39.15	0.54	48.22	0.66	0.12

Table 3. Apparent dilatancy angle and dilatancy index.

Vosges sandstone ¹⁰						
Confining pressure(MPa)	0.5	10	20	30	40	
Dilatancy angle ($^{\circ}$)	83.0	74.0	69.3	31.3	- 11.9	
Dilatancy index	1.00	0.89	0.83	0.37	- 0.14	
Gebdykes dolomite ³⁹						
Confining pressure(MPa)	0	5	20	40	90	
Dilatancy angle ($^{\circ}$)	87.3	83.0	51.1	60.7	3.4	
Dilatancy index	1.00	0.95	0.59	0.70	0.04	
Soft rock / Hard soil ³⁷						
Confining pressure(MPa)	0	0.2	0.5	1.0	2.0	
Dilatancy angle ($^{\circ}$)	65	61.7	50.7	26.6	1.7	
Dilatancy index	1.00	0.95	0.78	0.41	0.03	
Mudstone ⁴⁰						
Confining pressure(MPa)	5	10	15	30		
Dilatancy angle ($^{\circ}$)	75.3	68.2	46.9	36.5		
Dilatancy index	0.84	0.76	0.52	0.41		
Marble (conventional triaxial loading) ³⁵						
Confining pressure(MPa)	0	5	10	15	20	30
Dilatancy angle ($^{\circ}$)	85.70	78.96	75.72	75.55	66.27	64.87
Dilatancy index	1.00	0.9214	0.8816	0.8826	0.7733	0.7562
Marble (cyclic loading and unloading) ³⁵						
Confining pressure(MPa)	0	5	10	15	20	30
Dilatancy angle ($^{\circ}$)	85.79	78.86	75.63	75.98	71.47	73.11
Dilatancy index	1.00	0.9192	0.8816	0.8856	0.8330	0.821
The difference of marble dilatancy index between two different test schemes		0.022	0	0.03	0.0597	0.0648
Marble (unloading confining pressure) ⁴¹						
Confining pressure(MPa)	0	25	50	80		
Dilatancy angle ($^{\circ}$)	86.42	79.24	70.16	65.05		
Dilatancy index	1	0.92	0.81	0.75		
Drilling quartz mica schist parallel to the joint direction (unloading confining pressure) ⁴²						
Confining pressure(MPa)	0	30	40	50	60	
Dilatancy angle ($^{\circ}$)	73.36	21.88	60.34	53.84	47.08	
Dilatancy index	1	0.30	0.82	0.73	0.64	
Drilling quartz mica schist perpendicular to the joint direction (unloading confining pressure) ⁴²						
Confining pressure(MPa)	0	30	40	50	60	
Dilatancy angle ($^{\circ}$)	80.58	42.04	37.43	34.45	25.67	
Dilatancy index	1	0.52	0.46	0.43	0.32	

Table 4. Dilatancy indexes of different rocks under different test conditions.

It can be known from Table 4 that under both conventional triaxial loading and unloading confining pressure conditions, the dilatancy indicators of different rocks are all related to the confining pressure. Reference¹⁰ proposed a negative exponential relationship between the dilatancy index I_d and the confining pressure σ_3 :

$$I_d = k \exp(-m_d \sigma_3) \quad (8)$$

Where σ_{d0} is the minimum confining pressure without dilatancy phenomenon; k is a constant; m_d is the fitting parameter, which controls the curvature of the function and is determined by the experimental data.

The negative exponential function relationship curve of dilatancy index and confining pressure in conventional triaxial loading test and unloading confining pressure test is shown in Fig. 15. The correlation coefficient R^2 of negative exponential function obtained from unloading confining pressure test data is greater than that in conventional triaxial loading test, indicating that the relationship (8) is more suitable for unloading confining pressure test. When the confining pressure is between 0 and 15 MPa, the difference in the dilatancy index of coarse sandstone under the two test schemes is very small, only 0.02 or 0.03. When the confining pressure is between 15 and 20 MPa, the dilatancy index differences of coarse sandstone under the two test schemes are relatively large, which are 0.22 and 0.12 respectively. The differences in the dilatancy index of marble also show the same pattern (see Table 4). When the confining pressure is between 0 and 15 MPa, the differences in the dilatancy index of marble under the two test schemes are very small, only 0, 0.02 and 0.03. When the confining pressure is between 15 and 20 MPa, the difference in the dilatancy index of marble under the two test schemes is relatively large, which is 0.0597 and 0.0648 respectively. When the confining pressure is between 15 and 20 MPa, the dilatancy index is slightly larger due to the cyclic loading and unloading test scheme adopted for marble. Therefore, the difference in dilatancy index of marble is smaller than that of coarse sandstone.

The above experimental phenomena indicate that the loading method has a significant influence on rock dilatancy. The greater the confining pressure, the more significant the dilatancy of the rock mass during unloading. The confining pressure of 15 MPa may be a critical point that affects the dilatancy behavior of rocks. When the confining pressure in the roadway is greater than 15 MPa, the deformation of the rock mass will be more significant and the stability of the surrounding rock will be worse. This analytical method has certain guiding significance for the study of the stability of surrounding rock.

Characteristic stress threshold and corresponding strain

Characteristic stress threshold

The fracture initiation stress σ_{ci} , damage stress σ_{cd} and peak strength σ_p of rock are three important stress thresholds, which are the dividing points of different stages in the process of rock deformation and failure. The linear elastic stage, slow relative dilatancy stage and accelerated relative dilatancy stage of the volume strain curve of the rock sample with zero confining pressure (uniaxial loading) are not significant. Therefore, the initiation stress and damage stress of the rock sample C0 and its corresponding strain are not considered for the time being.

In the conventional triaxial loading test, the initiation stress, peak strength and residual strength all increase with the increase of confining pressure. It can be known through linear fitting that the above three characteristic stress thresholds show a strong linear correlation with the confining pressure, and the correlation coefficient is greater than 0.983 (see Fig. 16). Among them, the correlation coefficient of the peak intensity reached 0.9996, approaching 1. The damage stresses of rock samples C15 and C20 are basically equal (see Table 5), but generally increase with the increase of confining pressure. When the confining pressure increased from 5 MPa to 25 MPa, the crack initiation stress increased from 7.77 to 23.87 MPa, increasing by 3.07 times. The damage stress increased from 18.36 MPa to 66.85 MPa, an increase of 3.64 times. The peak strength increased from 32.84 MPa to 85.86 MPa, an increase of 2.61 times. The residual strength increased from 5.95 MPa to 26.77 MPa, an increase of 4.50 times.

In the unloading confining pressure test, the crack initiation stress, damage stress, peak strength and residual strength increase with the increase of confining pressure., it can be known through linear fitting that the above four characteristic stress thresholds show a good linear correlation with confining pressure, and the correlation coefficient is greater than 0.922. When the confining pressure increased from 5 MPa to 25 MPa, the crack initiation stress increased from 6.29 MPa to 21.81 MPa, increasing by 3.47 times. The damage stress increased from 15.25 MPa to 50.27 MPa, an increase of 3.29 times. The peak strength increased from 26.04 MPa to 68.81 MPa, an increase of 2.64 times. The residual strength increased from 3.52 MPa to 13.91 MPa, an increase of 3.95 times.

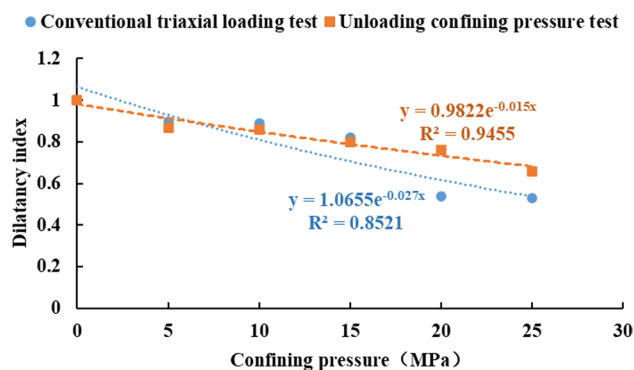
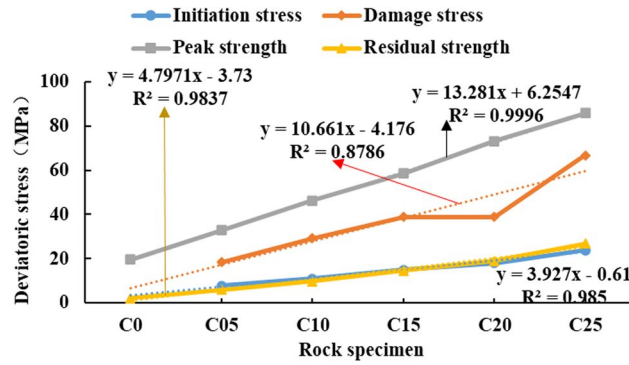
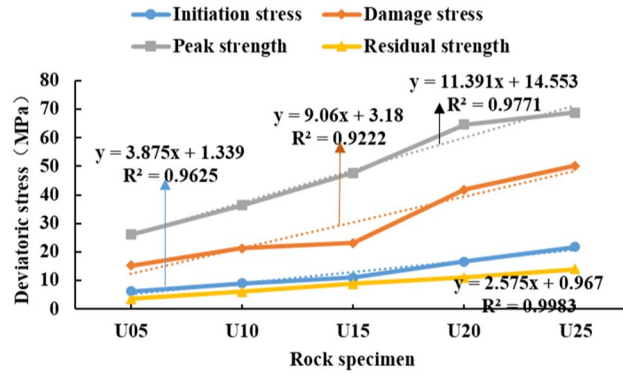


Fig. 15. The negative exponential relationship between confining pressure and dilatancy index.



(a) Conventional triaxial loading test



(b) Unloading confining pressure test

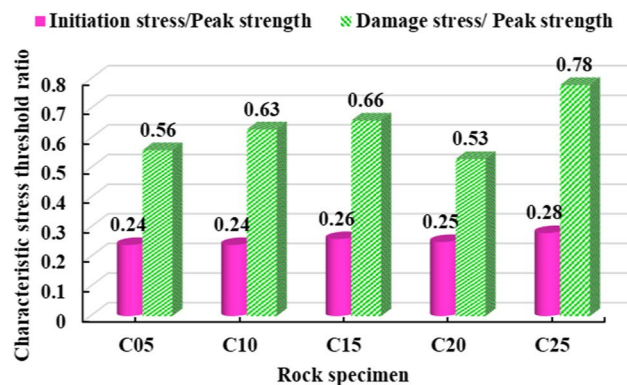
Fig. 16. Variation trend of characteristic stress threshold.

Rock specimen	Initiation stress(MPa)	Damage stress(MPa)	Peak strength(MPa)	Residual strength (MPa)
C0	—	—	19.59	2.07
C05	7.77	18.36	32.84	5.95
C10	10.89	29.34	46.34	9.77
C15	15	38.82	58.52	14.69
C20	17.96	38.97	73.27	19.11
C25	23.87	66.85	85.86	26.77
U05	6.29	15.25	26.04	3.52
U10	8.95	21.26	36.34	6.07
U15	11.11	23.20	47.73	8.92
U20	16.66	41.82	64.71	11.04
U25	21.81	50.27	68.81	13.91

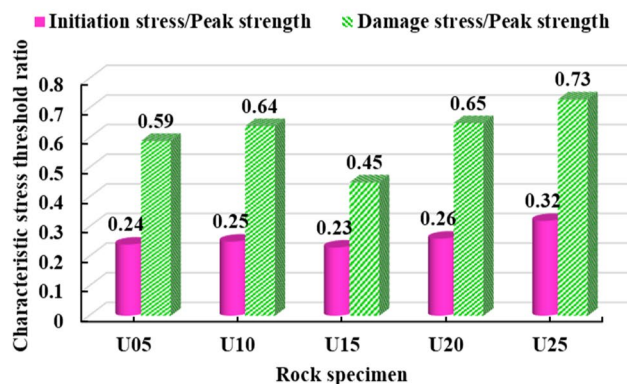
Table 5. Characteristic stress threshold.

From the above experimental phenomena, it can be known that in the loading and unloading tests, the confining pressure has the greatest influence on the residual strength, and its value has increased by approximately four times or more. Secondly, there are the crack initiation stress and damage stress, whose values have increased by approximately more than three times. The last one is the peak intensity, whose value has increased by approximately 2.6 times or more.

It can be known from the analysis of Fig. 17a that in the conventional triaxial loading test, σ_{ci}/σ_p and σ_{cd}/σ_p are respectively within the ranges of 0.53–0.78 and 0.24–0.28. As shown in Fig. 17b, it can be known that σ_{ci}/σ_p and σ_{cd}/σ_p are respectively within the ranges of 0.45–0.73 and 0.23–0.32 in the unloading confining pressure test. Combined with the characteristic stress threshold and its ratio variation law, the deformation and failure of rocks with different confining pressures can be predicted.



(a) Conventional triaxial loading test



(b) Unloading confining pressure test

Fig. 17. Variation trend of characteristic stress threshold ratio.

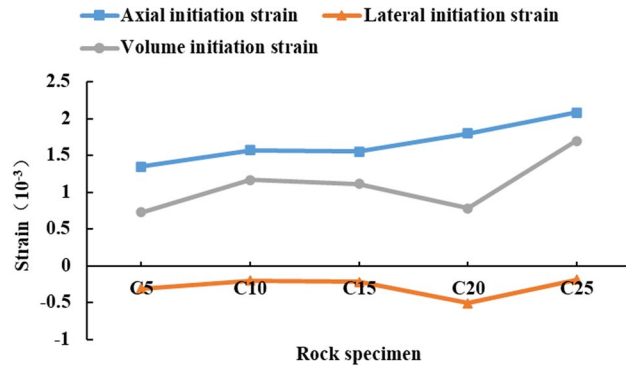
Characteristic strain threshold

(1) Crack initiation strain

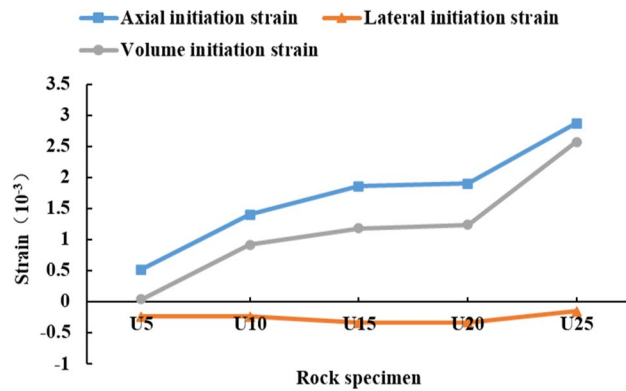
Studying the variation law of characteristic stress thresholds under different test conditions can predict the deformation and failure of rocks. As shown in Fig. 18, in the conventional triaxial loading test and unloading confining pressure test, the axial bursting strain and volume bursting strain generally increase with the increase of confining pressure, while the lateral bursting strain fluctuates slightly with the increase of confining pressure. As shown in Table 6, when the confining pressure increased from 5 to 25 MPa, the axial initiation strain in the conventional triaxial loading test increased from 0.00135 to 2.08, an increase of 1.54 times. The volume initiation strain increased from 0.0073 to 0.0017, an increase of 2.32 times. The axial bursting strain in the unloading confining pressure test increased from 0.00052 to 0.00287, an increase of 5.52 times. The volume initiation strain increased from 0.00004 to 0.00257, an increase of 64.25 times. Because the absolute values of the axial initiation strain and the lateral initiation strain of the rock sample U05 in the unloading confining pressure test are relatively close. The volume initiation strain of the rock sample is small, which further leads to the volume initiation strain of the rock sample U25 being much greater than that of the rock sample U05. It can be known from the above test phenomena that the influence of confining pressure on the axial initiation strain and The volume initiation strain under unloading conditions is greater than that of the loading test.

(2) Damage strain

As shown in Fig. 19, The axial damage strain and volume damage strain generally increase with the increase of confining pressure in the conventional triaxial loading test and the unloading confining pressure test, while the lateral damage strain fluctuates slightly with the increase of confining pressure. As shown in Table 7, when the confining pressure increased from 5 to 25 MPa, the axial damage strain in the conventional triaxial loading test increased from 0.003 to 0.00518, an increase of 1.73 times. The volume damage strain increased from 0.0011 to 0.00324, an increase of 2.95 times. The axial damage strain in the unloading confining pressure test increased from 0.00202 to 0.00485, an increase of 2.4 times. The volume damage strain increased from 0.00034 to 0.00377, an increase of 11.09 times. It can be known from the above test phenomena that the influence of confining pressure on the axial volume damage strain under unloading conditions is greater than that of the loading test.



(a) Conventional triaxial loading test



(b) Unloading confining pressure test

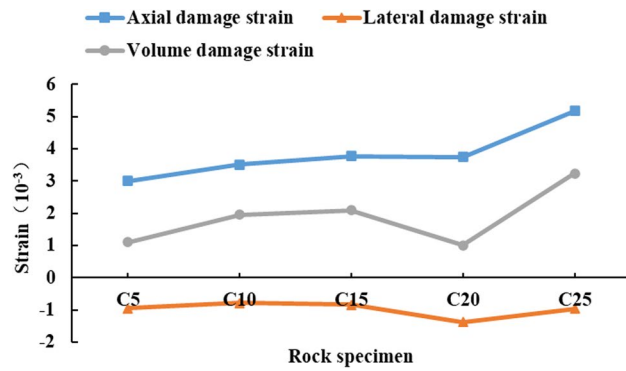
Fig. 18. The variation law of axial initiation strain, lateral initiation strain and volume initiation strain.

Rock specimen	Axial initiation strain(10 ⁻³)	Lateral initiation strain(10 ⁻³)	Volume initiation strain(10 ⁻³)
C0	—	—	—
C05	1.35	- 0.31	0.73
C10	1.57	- 0.2	1.17
C15	1.55	- 0.22	1.11
C20	1.8	- 0.51	0.78
C25	2.08	- 0.19	1.7
U05	0.52	- 0.24	0.04
U10	1.4	- 0.24	0.92
U15	1.86	- 0.34	1.18
U20	1.9	- 0.33	1.24
U25	2.87	- 0.15	2.57

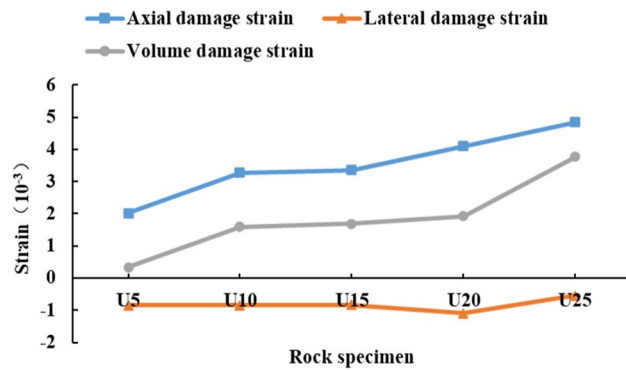
Table 6. Axial initiation strain, lateral initiation strain and volume initiation strain.

(3) Peak strain

As shown in Fig. 20, the axial peak strain, lateral peak strain and volume peak strain in the conventional triaxial loading test and the unloading confining pressure test generally increase linearly with the increase of confining pressure, and the correlation coefficient is above 0.9. As shown in Table 8, in the conventional triaxial loading test, with the increase of confining pressure, the axial peak strain increased from 0.00564 to 0.00804, increasing by 42.55%. The absolute value of the lateral peak strain decreased from 0.00629 to 0.00437, a reduction of 30.52%. The absolute value of the volume peak strain decreased from 0.00694 to 0.00071, a reduction of 89.77%. In the unloading confining pressure test, with the increase of confining pressure, the axial peak strain increased from 0.00574 to 0.00765, an increase of 33.28%. The absolute value of lateral peak strain decreased from 0.00606 to 0.00459, which decreased by 24.28%. The absolute value of the peak volume strain decreased from 0.00638 to 0.00153, a decrease of 76.02%. It can be known from the above test phenomena that the confining pressure has a



(a) Conventional triaxial loading test



(b) Unloading confining pressure test

Fig. 19. The variation law of axial damage strain, lateral damage strain and volume damage strain.

Rock specimen	Axial damage strain(10^{-3})	Lateral damage strain(10^{-3})	Volume damage strain(10^{-3})
C0	—	—	—
C05	3	- 0.95	1.1
C10	3.51	- 0.78	1.95
C15	3.77	- 0.84	2.09
C20	3.75	- 1.37	1.01
C25	5.18	- 0.97	3.24
U05	2.02	- 0.84	0.34
U10	3.27	- 0.84	1.59
U15	3.35	- 0.83	1.69
U20	4.1	- 1.09	1.92
U25	4.85	- 0.54	3.77

Table 7. Axial damage strain, lateral damage strain and volume damage strain.

significant influence on the volume peak strain in the loading and unloading tests. When the confining pressure is the same, the peak volume strain of unloading confining pressure is greater than that of the conventional triaxial loading.

(4) Residual strain

As shown in Fig. 21, the axial residual strain, lateral residual strain and volume residual strain in the conventional triaxial loading test and the unloading confining pressure test generally increase linearly with the increase of confining pressure, and the correlation coefficient is above 0.92. Among them, the volume peak strain showed a strong linear correlation with the confining pressure in the conventional triaxial loading test, with a correlation coefficient of 0.999, close to 1. As shown in Table 9, in the conventional triaxial loading test, with the increase of confining pressure, the axial residual strain increased from 0.00603 to 0.00862, increasing by 42.95%. The absolute value of the lateral residual strain decreased from 0.00712 to 0.0048, a reduction of 32.58%. The absolute value of the volume residual strain decreased from 0.00821 to 0.00098, a reduction of 88.06%. In the unloading

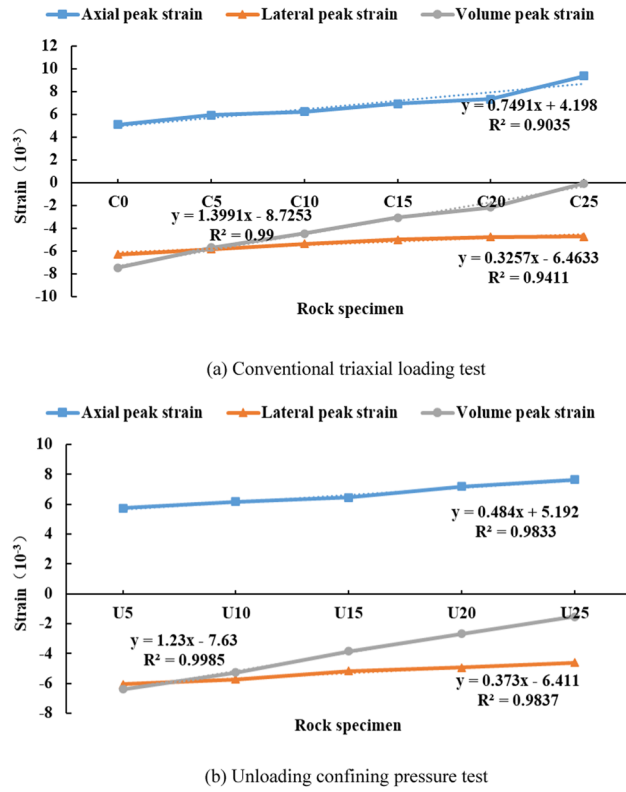


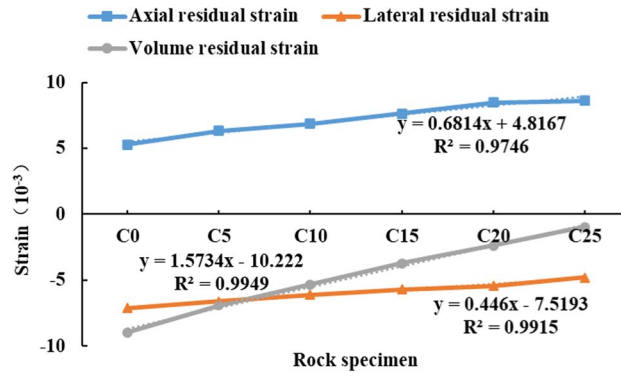
Fig. 20. The variation law of axial peak strain, lateral peak strain and volume peak strain.

Rock specimen	Axial peak strain(10 ⁻³)	Lateral peak strain(10 ⁻³)	Volume peak strain(10 ⁻³)
C0	5.11	- 6.29	- 7.47
C05	5.93	- 5.82	- 5.71
C10	6.24	- 5.35	- 4.46
C15	6.94	- 5.01	- 3.08
C20	7.32	- 4.75	- 2.18
C25	9.38	- 4.72	- 0.07
U05	5.74	- 6.06	- 6.38
U10	6.17	- 5.72	- 5.27
U15	6.47	- 5.16	- 3.85
U20	7.19	- 4.93	- 2.67
U25	7.65	- 4.59	- 1.53

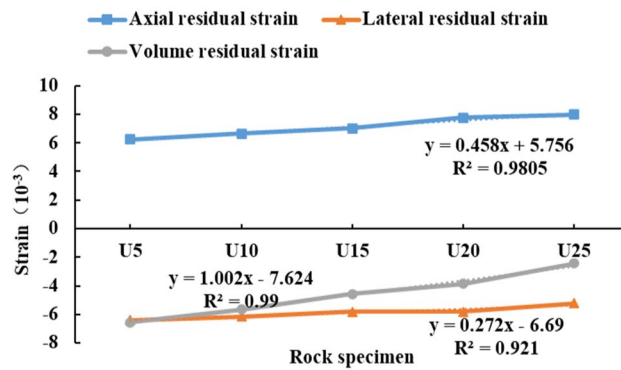
Table 8. Axial peak strain, lateral peak strain and volume peak strain.

confining pressure test, with the increase of confining pressure, the axial residual strain increased from 0.00624 to 0.00798, an increase of 27.88%. The absolute value of lateral residual strain decreased from 0.0064 to 0.00521, which decreased by 18.59%. The absolute value of the volume residual strain decreased from 0.00656 to 0.00244, which decreased by 62.80%. It can be known from the above test phenomena that the confining pressure has a significant influence on the volume residual strain in the loading and unloading tests. When the confining pressure is the same, the volume residual strain of unloading confining pressure is greater than that of conventional triaxial loading.

In summary, the variation ranges of volume crack initiation strain, volume damage strain, volume peak strain and volume residual strain in conventional triaxial loading test and unloading confining pressure test are greater than the corresponding axial strain and lateral strain, and all kinds of volume strains increase with the increase of confining pressure. In addition, the volume strain is determined by the axial strain and the lateral strain, and a slight change in either the axial strain or the lateral strain will alter the value of the volume strain. Therefore, the stress environment has a significant impact on the dilatancy capacity of rocks.



(a) Conventional triaxial loading test



(b) Unloading confining pressure test

Fig. 21. Variation trends of axial residual strain, lateral residual strain and volume residual strain.

Rock specimen	Axial residual strain(10 ⁻³)	Lateral residual strain(10 ⁻³)	volume residual strain(10 ⁻³)
C0	5.29	- 7.12	- 8.95
C05	6.32	- 6.62	- 6.92
C10	6.87	- 6.10	- 5.33
C15	7.65	- 5.69	- 3.73
C20	8.46	- 5.42	- 2.38
C25	8.62	- 4.80	- 0.98
U05	6.24	- 6.40	- 6.56
U10	6.65	- 6.15	- 5.65
U15	7.03	- 5.80	- 4.57
U20	7.75	- 5.81	- 3.87
U25	7.98	- 5.21	- 2.44

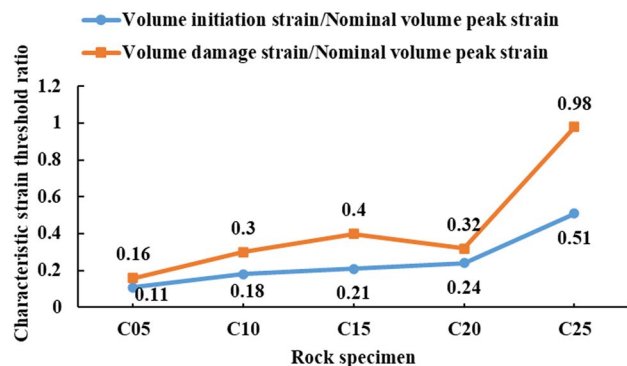
Table 9. Axial residual strain, lateral residual strain and volume residual strain values.

Volume strain threshold and volume strain at different dilatancy stages

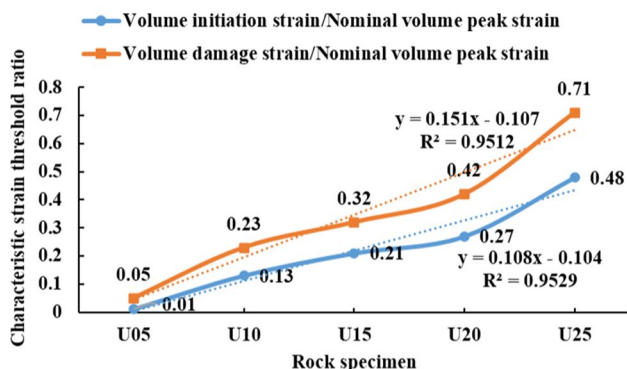
(1) The ratio of volume strain thresholds

The volume initiation strain, volume damage strain, volume peak strain and nominal volume peak strain are expressed by the letters ϵ_{vi} , ϵ_{vd} , ϵ_{vp} and ϵ_{nvp} , respectively, and $\epsilon_{nvp} = \epsilon_{vd} - \epsilon_{vp}$. As shown in Fig. 22a, in the conventional triaxial loading test, except for the $\epsilon_{vi}/\epsilon_{nvp}$ of rock sample C20 which decreased somewhat, the $\epsilon_{vi}/\epsilon_{nvp}$ of the remaining rock samples increased with the increase of confining pressure. The $\epsilon_{vd}/\epsilon_{nvp}$ of all rock samples increased with the increase of confining pressure. As shown in Fig. 22b, in the unloading confining pressure test, both $\epsilon_{vi}/\epsilon_{nvp}$ and $\epsilon_{vd}/\epsilon_{nvp}$ increase linearly with the increase of confining pressure.

(2) Proportion of volume strain in different dilatancy stages.



(a) Conventional triaxial loading test



(b) Unloading confining pressure test

Fig. 22. Variation trend of characteristic strain threshold ratio.

Rock specimen	Linear elastic stage	Slow relative dilatancy stage	Accelerated relative dilatancy stage	Absolute dilatancy stage	Accelerated relative dilatancy stage + Absolute dilatancy stage
C05	7.96	4.10	12.06	75.88	87.94
C10	12.67	8.45	21.13	57.75	78.88
C15	14.03	12.39	26.42	47.16	73.58
C20	17.73	5.23	22.95	54.09	77.04
C25	22.79	20.64	43.43	13.14	56.57
U05	0.55	4.14	46.96	90.61	95.30
U10	10.42	7.59	18.01	63.99	81.99
U15	14.84	6.42	21.26	57.48	78.74
U20	16.08	8.82	24.90	50.19	75.10
U25	25.75	12.02	37.78	24.45	62.22
Average value	14.29	8.98	23.26	53.47	76.74

Table 10. Volume strain ratio % in different dilatancy stages.

It can be known from Table 10 that, on the whole, the deformation amount of the rock is the largest in the absolute dilatancy stage, and the average proportion of volume strain is 53.47%. The second is the accelerated relative dilatancy stage, and the average proportion of volume strain is 23.26%. The proportion of volume strain in the accelerated relative dilatancy stage plus the absolute dilatancy stage was 56.57%-95.30%, and the average proportion of volume strain was 76.73%. When the eccentric stress exceeds the damage strength of the rock, the lateral strain begins to increase significantly, causing the volume strain to increase accordingly. Therefore, the volume strain in the above two dilatancy stages accounts for the vast majority of the four dilatancy stages.

The proportion of volume strain of the rock in the slow relative dilatancy stage accounts for the smallest, and the average proportion of volume strain is 8.98%. The second is the linear elastic stage, and the average proportion of volume strain is 14.29%. In the linear elastic stage and the slow relative dilatancy stage, the lateral strain is relatively small, and the crack begins to sprout but do not penetrate, resulting in a small proportion of

volume strain. The proportion of volume strain in different stages shows the accuracy of the division of rock dilatancy stages in this paper.

Conclusion

- (1) The conventional triaxial compression test and unloading confining pressure test of coarse sandstone were carried out. The differences and connections between volume strain and dilatancy were expounded, and the calculation formulas of volume strain in different deformation stages of rock were clarified. The rock dilatancy behavior is divided into four stages by using the deviatoric stress-volume strain curve, namely the linear elasticity stage, the slow relative dilatancy stage, the accelerated relative dilatancy stage and the absolute dilatancy stage. The concepts of relative dilatancy (broad dilatancy) and absolute dilatancy (narrow dilatancy) were proposed.
- (2) The relationship between rock dilatancy and confining pressure was described, and the variation laws of the apparent dilatancy angle and dilatancy index were illustrated by using the bilinear dilatancy model. In the conventional triaxial compression test and the unloading confining pressure test, the decrease rates of the apparent dilatancy angle were 40.79% and 23.99% respectively, and there was a negative exponential relationship between the dilatancy index and the confining pressure.
- (3) In the conventional triaxial loading test and unloading confining pressure test, the crack initiation stress, damage stress, peak strength and residual strength all increase with the increase of confining pressure. The confining pressure has the greatest influence on the residual strength, and its value increases by approximately four times or more. Secondly, there are the crack initiation stress and damage stress, whose values have increased by approximately more than three times. The last one is the peak strength, whose value has increased by approximately 2.6 times or more.
- (4) The axial crack initiation strain, volume crack initiation strain, axial damage strain, volume damage strain, axial peak strain and axial residual strain are all positive (i.e., compression), which increase with the increase of confining pressure, and the compression amount has recently increased. The average proportion of volume strain in the accelerated relative dilatancy stage and the absolute dilatancy stage is 76.73%, and the rock dilatancy phenomenon mainly occurs in the above two stages.

Data availability

The data used to support the findings of this study are available from the corresponding author upon request.

Received: 5 June 2025; Accepted: 31 October 2025

Published online: 03 December 2025

References

1. Wu, S. C. *Rock Mechanics* 75–91 (Higher Education Press, 2021).
2. Cai, M. F. *Rock Mechanics and Engineering* 61–63 (Science, 2002).
3. Zhou, W. Y. *Advanced Rock Mechanics* 87–90 (Water Power, 1990).
4. Chen, Z. J. & Kang, W. F. Time-dependent dilatancy prior to rock failure and earthquakes. *Chin. J. Rock. Mech. Eng.* **2** (01), 11–21 (1983).
5. Bridgman, P. W. Volume changes in the plastic stages of simple compression. *Appl. Phys.* **20**, 1241–1251 (1949).
6. Chen, Z. J. et al. Measurement of dilatancy, creep, and relaxation of brittle rock using an 8000 kN multifunctional triaxial apparatus. *Chin. J. Rock. Mech. Eng.* **8** (02), 97–118 (1989).
7. Hao, X. J. et al. Effect of natural fracture and confining pressure on damage-dilatancy point of deep coal measures reservoir and acoustic emission identification. *J. China Univ. Min. Technol.* **52** (04), 648–659 (2023).
8. Kang, H. P. & Yi, K. Simulation study on dilatant and rheologic properties of soft rocks surrounding deep roadway and its application. *China Coal Soc.* **48** (01), 15–33 (2023).
9. Harrison, J. P. Application of the elemental degradation approach to problems in rock engineering. (2008).
10. Bésuelle, P., Desrués, J. & Raynaud, S. Experimental characterization of the localization phenomenon inside a Vosges sandstone in a triaxial cell. *Int. J. Rock. Mech. Min. Sci.* **37** (8), 1223–1237 (2000).
11. Li, K. et al. A laboratory-testing-based study on mechanical properties and dilatancy characteristics of deeply buried mudstone under different stress loading rates. *China Coal Soc.* **48** (09), 3360–3371 (2023).
12. Li, W. P. et al. Research on sandstone dilation behavior and non-coaxiality under different stress lode angle conditions. *China Coal Soc.* **48** (S1), 71–81 (2023).
13. Yin, G. Z. et al. Influence of intermediate principal stress on dilation and strength characteristics of sandstone. *China Coal Soc.* **42** (04), 879–885 (2017).
14. Su, C. D. & Zhang, Z. H. Analysis of plastic deformation and energy property of marble under pseudo-triaxial compression. *Chin. J. Rock. Mech. Eng.* **27** (02), 273–280 (2008).
15. Yang, Z. et al. Dilatancy and acoustic emission characteristics of rock salt in Variable-Frequency fatigue tests. *Rock. Mech. Rock. Eng.* **57** (12), 1–18 (2024).
16. Xing, W. et al. Experimental study on dilatancy behavior of soft rock under dynamic loading. *Int. J. Rock. Mech. Min. Sci.* **182**, 1–12 (2024).
17. Li, P. et al. Elastic-plastic analysis of rock surrounding a circular roadway considering plastic hardening and dilatancy characteristics. *Sci. Rep.* **15** (1), 1–10 (2025).
18. Ping, Y., Li, S. C. & Wang, L. Experimental study of post-peak deformation of sandstone with pre-existing transfixion joint and its application in tunnel support. *China Coal Soc.* **39** (04), 644–650 (2014).
19. Meng, Q. B. et al. Experimental study on rock strength and deformation characteristics under triaxial cyclic loading and unloading conditions. *Rock. Mech. Rock. Eng.* **54**, 777–797 (2021).
20. Xu, H. F. et al. Volumetric strain of rock salt under triaxial low-frequency cyclic loading. *Chin. J. Geotech. Eng.* **37** (04), 741–746 (2015).
21. Lu, X. L. & Liu, Q. S. Constitutive model of rocks considering dilatancy-bulking behaviour and its calibration. *Chin. J. Rock. Mech. Eng.* **32** (09), 1886–1893 (2013).

22. Zhao, X. G. et al. Damage and dilation characteristics of deep granite at Beishan under Cyclic loading-unloading conditions. *Chin. J. Rock. Mech. Eng.* **33** (09), 1740–1748 (2014).
23. Hou, W. S. et al. Comparison between dilatancy onset and peak of different rocks. *Chin. J. Geotech. Eng.* **35** (08), 1478–1485 (2013).
24. Zhang, C. S. et al. Mechanical behaviors of basalt at Baihetan hydropower station and simulation with Hoek-Brown constitutive model. *Chin. J. Rock. Mech. Eng.* **38** (10), 1964–1978 (2019).
25. Li, C. B., Xie, H. P. & Xie Experimental and theoretical study on the shale crack initiation stress and crack damage stress. *China Coal Soc.* **42** (04), 969–976 (2017).
26. Huang, W., Shen, M. R. & Zhang, Q. Z. Study of unloading dilatancy property of rock and its constitutive model under high confining pressure. *Chin. J. Rock. Mech. Eng.* **29** (S2), 3475–3481 (2010).
27. Liu, H. X. et al. Mechanical response and dilatancy characteristics of deep marble under different stress paths: A sight from energy dissipation. *Cent. South. Univ.* **31** (6), 2070–2086 (2024).
28. Zhou, H. et al. Characteristics and mechanism of occurrence of stress thresholds and corresponding strain for hard rock. *Chin. J. Rock. Mech. Eng.* **34** (08), 1513–1521 (2015).
29. Cai, M. et al. Generalized crack initiation and crack damage stress thresholds of brittle rock masses near underground excavations. *Int. J. Rock. Mech. Min. Sci.* **41** (5), 833–847 (2004).
30. Shan, H. Z. *Mechanics of materials* (2nd ed.). *High. Educ. Press.*, 219–222. (2022).
31. Xu, Z. L. *Elasticity* 4th edn, 197–199 (Higher Education Press, 2022).
32. Wu, J. L. *Elasticity* (3rd ed.). *High. Educ. Press.*, 36–40. (2019).
33. Zhang, R. et al. Fractal analysis of acoustic emission during uniaxial and triaxial loading of rock. *Int. J. Rock. Mech. Min. Sci.* **79**, 241–249 (2015).
34. Chen, Z. H., Fu, Y. F. & Tang, C. A. Confining pressure effect on the acoustic emission during rock failure. *Chin. J. Rock. Mech. Eng.* **16** (01), 66–71 (1997).
35. Yu, J. et al. Characteristics of dilatancy of marble under variable amplitude Cyclic loading and unloading. *Rock. Soil. Mech.* **42** (11), 2934–2942 (2021).
36. Fang, Z. & Harrison, J. P. A mechanical degradation index for rock. *Int. J. Rock. Mech. Min. Sci.* **38** (8), 1193–1199 (2001).
37. Yuan, S. C. & Harrison, J. P. An empirical dilatancy index for the dilatant deformation of rock. *Int. J. Rock. Mech. Min. Sci.* **41** (4), 679–686 (2004).
38. Yang, Y. R. et al. Dilatancy and energy characteristics analysis of transverse-isotropic rock mass under triaxial unloading condition. *Rock. Soil. Mech.* **38** (06), 1589–1599 (2017).
39. Santarelli, F. J. Theoretical and experimental investigation of the stability of the axisymmetric wellbore. PhD thesis, University of London (1987).
40. Zhang, C. K. & Li, L. F. Study on relation between rock post-peak dilatancy and confining pressure. *Non-ferrous Met.* **61** (04), 134–137 (2009).
41. Liu, X. H. et al. Dilatancy characteristics and crack evolution of deep-buried marble under unloading confining pressure. *Undergr. Space Eng.* **18** (06), 1922–1932 (2022).

Author contributions

Yanhong Du wrote the main manuscript text. Feng Chen prepared Figs. 1, 2, 3, 4, 5, 6, 7 and 8. All authors reviewed the manuscript.

Funding

The laboratory test was supported by the National Natural Science Foundation of China (52474228).

Declarations

Competing interests

The authors declare no competing interests.

Additional information

Correspondence and requests for materials should be addressed to Y.D.

Reprints and permissions information is available at www.nature.com/reprints.

Publisher's note Springer Nature remains neutral with regard to jurisdictional claims in published maps and institutional affiliations.

Open Access This article is licensed under a Creative Commons Attribution-NonCommercial-NoDerivatives 4.0 International License, which permits any non-commercial use, sharing, distribution and reproduction in any medium or format, as long as you give appropriate credit to the original author(s) and the source, provide a link to the Creative Commons licence, and indicate if you modified the licensed material. You do not have permission under this licence to share adapted material derived from this article or parts of it. The images or other third party material in this article are included in the article's Creative Commons licence, unless indicated otherwise in a credit line to the material. If material is not included in the article's Creative Commons licence and your intended use is not permitted by statutory regulation or exceeds the permitted use, you will need to obtain permission directly from the copyright holder. To view a copy of this licence, visit <http://creativecommons.org/licenses/by-nc-nd/4.0/>.

© The Author(s) 2025